

Article

Chemical and Microstructural Properties of Fly Ash and Fly Ash/Slag Activated by Waste Glass-Derived Sodium Silicate

Dali Bondar ^{1,*}  and Raffaele Vinai ²¹ Material Evolution Ltd., Materials Processing Institute, Middlesbrough TS6 6US, UK² College of Engineering, Mathematics and Physical Sciences, University of Exeter, Exeter EX4 4QF, UK; r.vinai@exeter.ac.uk

* Correspondence: dlbondar@gmail.com; Tel.: +44-(0)-7742-756044

Abstract: Sodium silicate is commonly used for activating alumina silicates to produce alkali-activated binders that can compete with conventional Portland cement in concrete. However, the cost and emissions related to activators can hinder the use of alkali-activated materials in the industry. The novel, waste-based activators have been developed in the last years, using Si-rich waste streams. Processing waste glass cullet not only reduces the glass landfill disposal but also allows the production of sodium silicate for alkali activation. In this article, the chemical and microstructural properties of neat fly ash and blended 60 fly ash/40 slag pastes activated by sodium silicate produced from glass cullet were studied and compared to equivalent ones activated by commercially available sodium silicate and sodium hydroxide solutions. Fourier transform infrared (FTIR) spectroscopy, X-ray powder diffraction (XRD), thermogravimetric analysis (TGA) and scanning electron microscopy (SEM) coupled with energy dispersive X-ray (EDX) were used to determine the microstructure and composition of the gel phase. Findings have confirmed that pastes activated by the processed waste glass showed chemical and microstructural properties comparable to pastes produced with commercially available activators.

Keywords: alkali activated fly ash and fly ash/slag; waste glass; sodium silicate; microstructural properties; fourier transform infrared (FTIR) spectroscopy; X-ray powder diffraction (XRD); thermogravimetric analysis (TGA); scanning electron microscopy (SEM)



Citation: Bondar, D.; Vinai, R. Chemical and Microstructural Properties of Fly Ash and Fly Ash/Slag Activated by Waste Glass-Derived Sodium Silicate. *Crystals* **2022**, *12*, 913. <https://doi.org/10.3390/cryst12070913>

Academic Editor: Zhaohui Li

Received: 29 May 2022

Accepted: 23 June 2022

Published: 27 June 2022

Publisher's Note: MDPI stays neutral with regard to jurisdictional claims in published maps and institutional affiliations.



Copyright: © 2022 by the authors. Licensee MDPI, Basel, Switzerland. This article is an open access article distributed under the terms and conditions of the Creative Commons Attribution (CC BY) license (<https://creativecommons.org/licenses/by/4.0/>).

1. Introduction

Almost eighty percent of 130 million tonnes of global production of glass each year are being discarded as waste while only 21% of the waste glass (WG) is recycled [1,2]. The waste glass has been investigated either as a substitution for binder (because of its pozzolanic properties) or as a replacement for aggregate in concrete. The substitution of concrete filler and aggregate with waste glass can be conducted considering its alkali silica reaction (ASR) properties [1,3]. Ke et al. showed that using waste glass with a particle size coarser than 300 µm and a substitution rate higher than 30% induces ASR expansion [4]. Siddika et al. reported that the ASR expansion issue is less critical for geopolymers compared with conventional concrete [1,2].

Due to its high content of amorphous silicates, waste glass is an ideal candidate for the production of low carbon binders from alumina silicates for alkali activated (sometimes referred to as geopolymer) concretes. To date, most of the studies that investigated the use of waste glass as a constituent of blended precursor for geopolymer concrete have shown that a substitution rate of 20% in binders reduces the shrinkage and improves the carbonation resistance [5–8]. A high-temperature process is, however, required for blended metakaolin-waste glass geopolymers [9]. Mácová et al. investigated the production of a metakaolin-based alkali-activated concrete containing waste foam glass. Samples with high porosity (>45%), a low thermal conductivity coefficient (<0.2 W/mK), and low mechanical

properties were obtained, suggesting the suitability of the mix for thermal-insulation applications [10].

Glass waste dissolved in NaOH (4 M) solution was used for soil treatment for brick production [11]. Sasui et al. used sieved WG powder dissolved in NaOH (4 M) solution in three different proportions, i.e., 10, 20 and 30 g per 100 mL of NaOH (4 M) solution to activate Class C fly ash/slag mixtures. The results showed that reactive Ca supplied from slag and the dissolved silica in the alkaline solution resulted in a homogeneous and compact matrix with low porosity and high mechanical strength [12]. Melele et al. investigated reactive hardeners from rice husk ash and waste glass separately prepared by adding NaOH pellets, mixing with distilled water and stirring the solution for 30 min at 100 °C, to manufacture metakaolin-based geopolymer samples. They found that the reactivity of waste glass solution can be improved by adding hardener from rice husk ash to produce geopolymer cement with higher compressive strengths, denser matrix, and a homogeneous and compact microstructure [13]. Bagheri and Moukannaa used a hydrothermal approach for the activation of WG and dissolved the WG in an alkaline medium at 65 °C for 2 h to produce a fly ash/slag blend based geopolymer with a 7-day compressive strength up to 28 MPa [14].

Vinai and Soutsos proposed a simple method to produce sodium silicate from WG. The effects of different process parameters, such as alkali ratio, temperature and water content on the product mineralogy were assessed and the efficiency of the developed activator product was investigated by comparing the compressive strength of fly ash/slag and fly ash-based mortar cubes activated with the WG-based sodium silicate, with the strength of samples produced with commercially available sodium hydroxide and sodium silicate [15]. WG-based activator gave lower early strength (1-day) but equal or superior 7 and 28-day strengths than the commercially available activating solutions. Since the method was proposed, it has been replicated and verified by several researchers (see, e.g., [16]), using other silicate sources (e.g., [17,18]), and providing environmental analysis confirming a potential for a 70% reduction in CO₂ emissions when compared to Portland cement-based concrete [19,20]. However, a detailed investigation of the microstructure of the reaction products when a WG-based activator is used has not been carried out yet.

This article describes the results of an investigation of the microstructure of alkali-activation reaction products obtained using the WG-derived sodium silicate proposed by Vinai and Soutsos. Paste samples manufactured with commercial sodium silicate as an activator for fly ash and fly ash/slag were also investigated and their microstructural features were compared to those of samples produced with a WG-based activator.

2. Materials and Experimental Methods

2.1. Materials and Paste Sample Specifications

The glass cullet used was from domestic glass bottles and supplied from Enva Toomebridge a local recycler in Belfast, Northern Ireland including glass chips of different colours and sizes. Glass waste was milled using a German Retsch PM400 Ball Mill, capable of grinding around 440 g of glass (110 g in each of the four pots loaded with 10 steel balls of 15 mm diameter) at a speed of 300 rpm each time. The D50 value (i.e., the value of the particle size at 50% in the cumulative distribution) showed that the fineness of the material was improved by the milling time. Milling time of 10 min resulted in an average powder dimension equal to 12 µm. Grinding the material for 10 min at 300 rpm was considered suitable and adopted in the study [15]. The oxide composition of the glass powder was obtained from the X-ray fluorescence test and presented in Table 1 [15].

Table 1. Oxide composition of the glass powder used in this study.

| Element | SiO ₂ | TiO ₂ | Al ₂ O ₃ | Fe ₂ O ₃ | MnO | MgO | CaO | Na ₂ O | K ₂ O | P ₂ O ₅ | SO ₃ | LOI | Total |
|----------|------------------|------------------|--------------------------------|--------------------------------|-------|------|-------|-------------------|------------------|-------------------------------|-----------------|------|-------|
| Mass (%) | 71.51 | 0.07 | 1.74 | 0.34 | 0.028 | 1.34 | 10.73 | 13.29 | 0.64 | 0.01 | 0.089 | 0.27 | 100.0 |

WG-based sodium silicate was produced following the method proposed by Vinai and Soutsos [15], mixing WG powder with NaOH prills at a mass ratio of 11:10, adding a small amount of water for the creation of a paste, and processing the paste in an oven at a temperature between 150 °C and 330 °C. Commercial grade sodium hydroxide (Atznatron caustic soda from AkzoNobel, Mainz, Germany) in micro prills was used for the reaction with the ground waste glass. The precursors used were ground granulated blast furnace slag (GGBS) and low-CaO fly ash, provided by ECOCEM—Ireland, Dublin, and Drax Power Minerals Ltd., Selby, North Yorkshire, UK, respectively. The grain size of fly ash was in the range of 0.24–105 µm. The crystalline phases detected in fly ash were mainly Mullite, Quartz and traces of Hematite, whereas the amorphous content was about 85%. GGBS grain size was in the range 0.24–149 µm, and its nature was mainly (>90%) amorphous, showing minor traces of Akermanite and Gehlenite. The oxide composition of these materials was obtained from the X-ray fluorescence test, and it is shown in Table 2.

Table 2. Oxide compositions and particle size of GGBS and fly ash.

| Precursor | Component (Mass% as Oxide) | | | | | | | | | | | Particle Size (%) |
|-----------|----------------------------|--------------------------------|------|--------------------------------|-----|-------------------|------------------|------------------|-----------------|--------|------|-------------------|
| | SiO ₂ | Al ₂ O ₃ | CaO | Fe ₂ O ₃ | MgO | Na ₂ O | K ₂ O | TiO ₂ | SO ₃ | Others | LOI | Fineness ≥ 45 µm |
| GGBS | 35.7 | 11.2 | 43.9 | 0.3 | 6.5 | 0.5 | 0.2 | 0.5 | 0.3 | 0.59 | 0.31 | 7.74 |
| Fly ash | 46.8 | 22.5 | 2.2 | 9.1 | 1.3 | 0.89 | 4.09 | 1.05 | 0.9 | 7.57 | 3.6 | 18.39 |

Commercially available sodium silicate solution (Fisher Scientific UK Ltd. with SiO₂ content of 25.5% and Na₂O content of 12.8%, i.e., SiO₂/Na₂O = 2) and a sodium hydroxide solution prepared by dissolving the Atznatron caustic soda in water at 30% mass concentration were used to produce control paste.

Two series of paste samples were produced, using a blend of 60%/40% fly ash/GGBS, as well as neat fly ash as a precursor. The alkali modulus (AM), i.e., the mass ratio Na₂O/SiO₂ was kept equal to 1.0, whereas the alkali dosage (M+), i.e., the percentage mass ratio Na₂O/binder, was kept equal to 7.5%. The water to solid ratio (w/s) was kept at 0.37 [15]. The WG-based powder activator was dissolved in the required water volume. In order to take into account the variability in the quality of the produced sodium silicate, mixes were manufactured dosing the WG-based activator, assuming an efficiency of 70% (i.e., increasing the quantity of material from the theoretical value), as well as an efficiency of 90%. The samples were prepared by mixing the powder and solution using a Hobart blender and pouring the paste into sealed plastic bags and kept under relevant environmental conditions (i.e., 70 °C oven curing for 100% fly ash, 20 °C for 60 fly ash/40 slag mixes) until the test date. Fractions of the samples were broken and milled in a pestle, and the obtained powders were used for FTIR, XRD and TGA analysis and some broken fractions were used for each SEM test. The pastes investigated in this study are summarised in Table 3.

Table 3. Paste code description.

| Paste Code | Description |
|------------|---|
| 60/40FG-70 | (60/40%) fly ash/GGBS paste with assumed efficiency of the silicate powder equal to 70% |
| 100F-70 | 100% fly ash paste with assumed efficiency of the silicate powder equal to 70% |
| 100F-90 | 100% fly ash paste with assumed efficiency of the silicate powder equal to 90% |
| FG-CON | Control pastes with commercial (Fisher sodium silicate, NaOH 30% solution) activators and (60/40%) fly ash/GGBS |
| F-CON | Control pastes with commercial (Fisher sodium silicate, NaOH 30% solution) activators and 100% fly ash |

2.2. Experimental Methods

Fourier transform infrared (FTIR) spectrometry was carried out using a Jasco 4100 series FTIR Spectrometer (wavenumber range 7800 to 350 cm^{-1}) recording data in transmittance mode over the range 650 to 4000 cm^{-1} , with a data interval of 0.964 cm^{-1} . Jasco software was used for data interpretation and deconvolution analysis.

X-ray diffraction (XRD) tests were carried out with a PANalytical X'Pert HighScore PRO diffractometer using pure Copper-K-Alpha 1 radiation with wavelength 1.54 Å. The X-ray generator was set to 40 kV and 40 mA, the recorded angular range was 5 to 65 or 70° (2 θ) with a step close to 0.017°. X-Pert HighScore software was used for data interpretation.

Thermogravimetric Analysis (TGA) was carried out on samples using a NETZSCH PERSEUS TG 209F1 Libra. A small amount of sample (10 \pm 1 mg) was tested at a controlled heating rate (temperature increase per unit of time, 20 °C/min) to observe the evolution of the sample mass vs. the temperature. The temperature range was from 30 °C to 900 °C. Furthermore, along with the data processing (post-experiment), the mass loss values were converted to percentages which allowed a coherent comparison between the different samples.

Scanning electron microscopy (SEM) with elemental analysis was carried out on polished or crushed paste samples with a gold-palladium coating. An accelerating voltage of 5 kV and a working distance of 10 mm was used for imaging. The equipment used was PHILIPS/FEI QUANTA FEG-250 with OXFORD X-Act as an energy dispersive X-ray (EDX) analyser, which was run by AZtec version 2.0 software for analysis.

3. Results and Discussion

3.1. FTIR Investigation on the Developed Activator and Activated Pastes

The FTIR test results for the commercially available sodium silicate, unprocessed and processed waste glass powders produced at different temperatures (150, 250 and 330 °C) are shown in Figure 1. The broad and strong absorption band at 999 cm^{-1} for unprocessed WG powder could be ascribed to stretch vibration of the Si-O-Si or Si-Bridge Oxygen (Si-BO) bond. In alkaline silicate activators, the peaks associated with the Si-O or Si-None Bridge Oxygen (Si-NBO) groups are in the band 675–1000 cm^{-1} which are reactive and can be dissolved and attend the geopolymer reaction. The commercial sodium silicate has shown three peaks in the band 675–850 cm^{-1} that could be attributed to Si-O and a broad and strong absorption band at 980 cm^{-1} ascribed to stretch vibration of Si-O-Na. All the three processed WG have shown sharp peaks at 880 and 960 cm^{-1} associated with Si-OH and Si-O-Na, respectively [21]. While the processed powder at 330 °C has shown a sharp peak around 1024 cm^{-1} and depicts asymmetric silicon which is insoluble. Even if the production of reactive sodium silicate proved to be successful at lower temperatures, this study investigated the powder produced at 330 °C as this resulted in the more pronounced peaks from FTIR tests [15].

Figure 2a details the FTIR spectra recorded in the range 1250–650 wavenumber for fly ash before and after activation with WG-based, as well as commercial activators, cured for 14 and 28 days. Before activation, the main peak was at 1042 cm^{-1} , which displays Si-O-Si stretching bands with several smaller peaks in the band 650–800 cm^{-1} . After activation, the band centred at 1042 cm^{-1} was shifted towards a lower wave number of about 980 cm^{-1} in 14-day cured samples, further shifted at about 989 cm^{-1} in 28-day cured samples. These bands are ascribed to stretch vibration of Si-O-Na and Si-O-Al bonds that are formed in neat fly ash geopolymer pastes with increasing alkali concentration, confirming the depolymerisation (i.e., dissolution from the precursor) of silicate and/or aluminosilicate structures in the fly ash. During alkali activation, every bridging oxygen atom (BO) on the surface of the original aluminosilicate is replaced by two negatively charged non-bridging oxygen atoms (NBO), which are charge compensated by alkalis. When all the polymerised alumina-silicate has dissolved, layered silicates with a few siloxyl groups are left in place. This corresponds to the measured stretching vibration at the wavenumber around 990 cm^{-1} , and its structure is exclusively formed by Si-O-Al bridges [22,23]. Assuming

that the area of the resolved bands is proportional to the concentration of the corresponding bonds, then more Si–O–Si and Si–O–Al bond formation can be found for mixes made with 100% fly ash activated by the WG-based activator than mixes made with commercial activators. The strength of Si–O–Si and Si–O–Al bonds could explain the higher compressive strength of the geopolymers activated with WG-based silicate observed in the previous study [15].

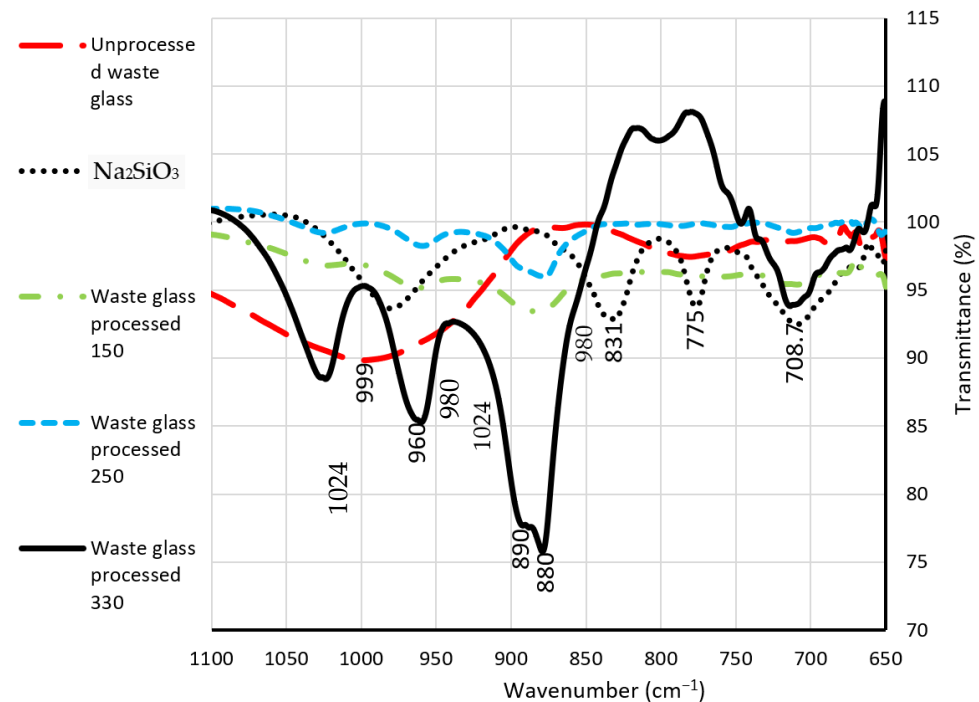


Figure 1. Detail of the 1100–650 wavenumber range for FTIR of commercially available Na_2SiO_3 , unprocessed waste glass powder and the processed ones at 150, 250 and 330 °C.

The infrared spectra of the fly ash and slag powders and hardened geo-polymeric samples manufactured with a 60/40% fly ash/slag blend and cured at room temperature after 14 and 28 days are shown in Figure 2b. In unreacted fly ash and slag powders, the maximum value of the broad peak was about 1042 cm^{-1} and 926 cm^{-1} , respectively. In the reacted samples, this peak has shifted towards $954\text{--}959\text{ cm}^{-1}$. The effect of slag inclusion in the mix can be observed by comparing the peak for activated neat fly ash ($978\text{--}989\text{ cm}^{-1}$, see Figure 2a) with the peak for mix with 60/40 fly ash/slag ($954\text{--}959\text{ cm}^{-1}$, see Figure 2b). The decrease is presumably due to the formation of C–S–H and C–A–S–H gels, associated with a reduction in the amount of Al [24]. FTIR results seem, therefore, to confirm that the activator developed from glass waste can depolymerise the original silicate and/or alumina-silicate structures and be used to activate the aluminosilicates.

3.2. XRD Analysis of the Activated Pastes

The XRD diffractograms (in the range of $5\text{--}65^\circ 2\theta$) of the activated pastes are shown in Figure 3. The XRD patterns of the mainly amorphous activated neat fly ash (Figure 3a) show that mullite ($\text{Al}_6\text{Si}_2\text{O}_{13}$), quartz (SiO_2), calcium aluminate (CaAl_2O_4), calcium aluminium silicate hydroxide $\text{Ca}_2\text{Al}_3(\text{SiO}_4)_3(\text{OH})$ and hematite (Fe_2O_3) are the main crystalline minerals detected. When observing the diffractograms obtained from the fly ash/slag blend (Figure 3b), calcium silicate hydrate ($\text{CaH}_2\text{O}_4\text{Si}$) can be observed instead of calcium aluminate. The sharp characteristic quartz, mullite, calcium aluminate and calcium silicate hydrate peaks are associated with the development of alkali-silicate glasses with the partial amorphisation of the phases. The crystalline phases (quartz, mullite and hematite) observed in the fly ash remained almost unchanged after synthesis and could be attributed

either to their non-participation in the reaction, as well as to the unreacted fly ash [14,20]. Furthermore, the broad halo observed between 20 and $35^\circ 2\theta$ for activated neat fly ash and between 22 and $38^\circ 2\theta$ for activated 60/40 fly ash/slag indicates the presence of amorphous N-A-S-H and C-A-S-H gels.

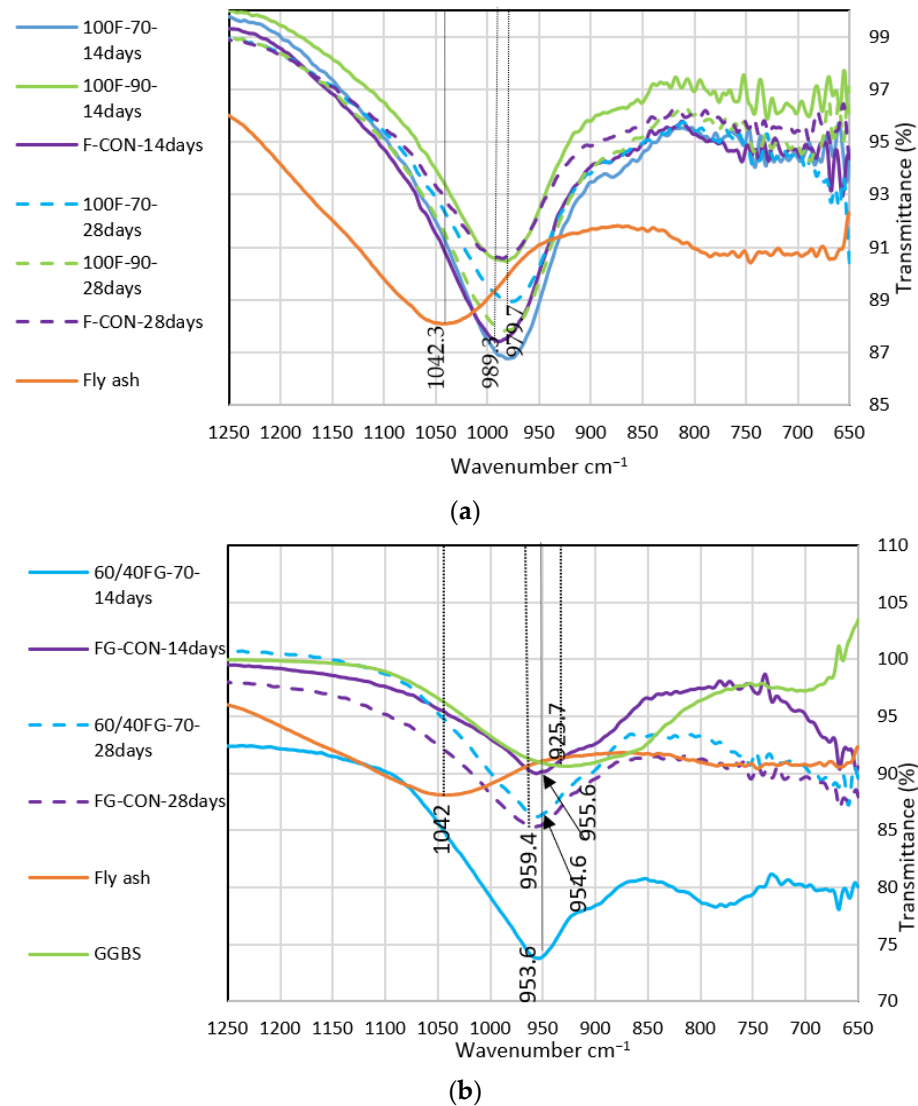


Figure 2. (a) FTIR of neat fly ash pastes activated with WG-based and commercially available activators at 14 and 28 days. Detail of the range $1250\text{--}650\text{ cm}^{-1}$. (b) FTIR of 60/40 fly ash/slag paste activated with WG-based and commercially available activators at 14 and 28 days. Detail in the range $1250\text{--}650\text{ cm}^{-1}$.

3.3. TGA Analysis of the Activated Pastes

Figure 4a, b show the results of the TGA analysis on the heat flow and percentage of weight loss of the activated neat fly ash 60/40 fly ash/slag samples.

All neat fly ash samples exhibit a remarkable mass loss before around 150°C while this is 100°C for 60% fly ash/40% slag samples. This is attributed to the loss of physically bound water within the paste. Endothermic peaks in the range of 141°C to 148°C for activated neat fly ash and 98°C to 107°C for activated fly ash/slag blend caused evaporation of the absorbed water typically observed in mineral materials. The higher endothermic peak at 148°C in the activated sample seems to suggest a slightly denser structure of the 100% fly ash mix produced with WG-based activator dosed by assuming an efficiency of 70% (i.e., samples with the highest volume of WG-based activator). This sample has shown

an evaporable water content of 4.5%, which is slightly higher than the one activated with the WG-based activator dosed by assuming an efficiency of 90%, as well as the sample produced with commercially available activators (2.6 and 2.4%, respectively).

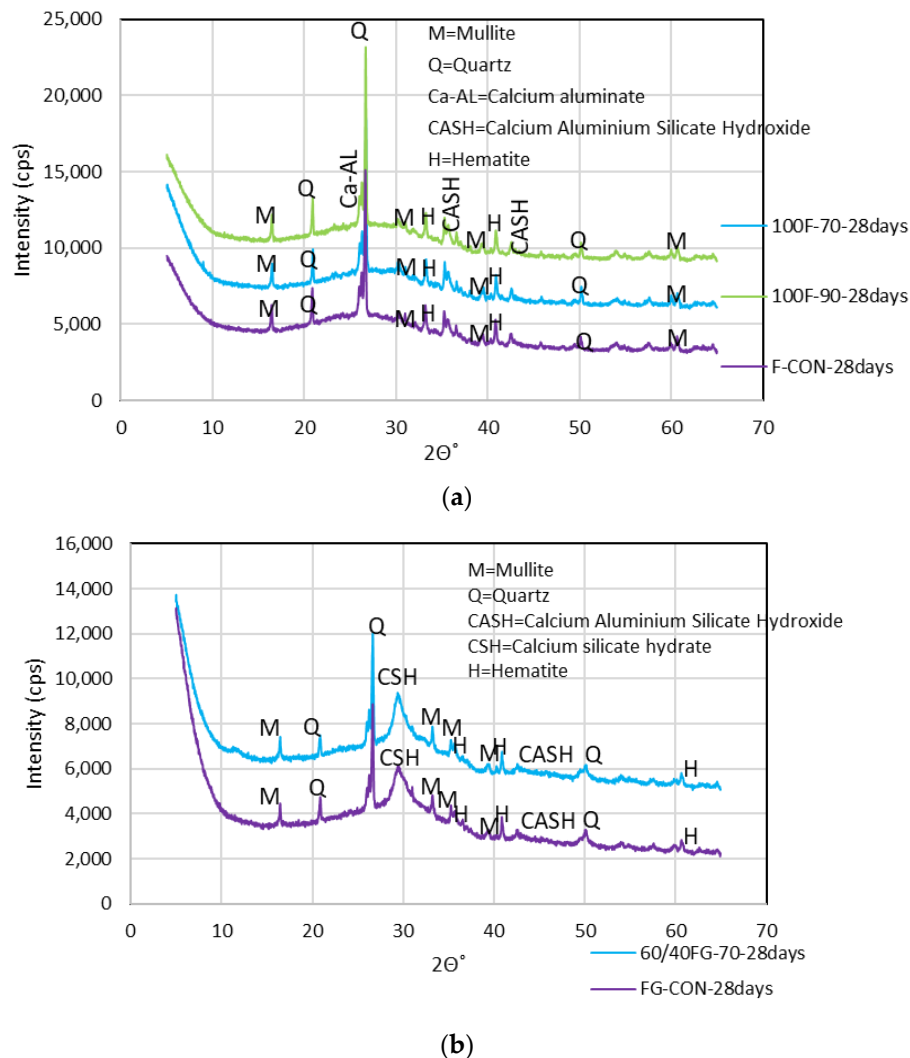


Figure 3. (a) XRD of neat fly ash activated with WG-based and commercially available activators at 28 days. (b) XRD of 60/40 fly ash/slag activated with WG-based and commercially available activators at 28 days.

After the evaporation of the physically bound water, all neat fly ash samples show a remarkable heat flow increasing at 150 to 300 °C, followed by a less steep increase until around 450 °C, while for activated fly ash/slag blend this behaviour was observed in the temperature range from 100 to 200 °C. After around 450 °C, all the activated neat fly ash mixes show a stable curve with limited mass loss observed for mixes made WG-based activator dosed assuming 70% efficiency. The activated fly ash/slag blend showed a stable curve after around 200 °C.

Between 400 °C and 830 °C, the mass loss of activated neat fly ash was slow and attributed to the thermal decomposition of the remaining carbon from unreacted fly ash; 100% fly ash mix produced with WG-based activator dosed at 70% efficiency showed a small change of the mass loss starting at 765 °C. A similar change was observed at 917 °C for mixes activated with commercially available activators.

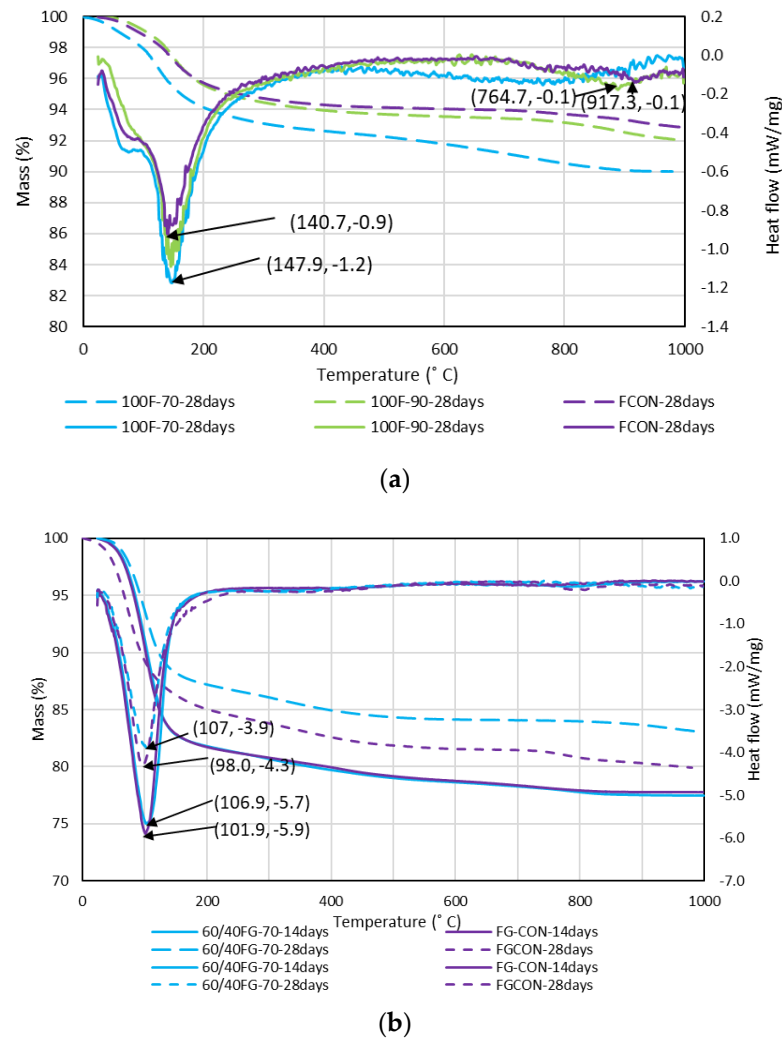


Figure 4. (a) TGA of neat fly ash activated with WG-based and commercially available activators at 28 days. (b) TGA of 60/40 fly ash/slag activated with WG-based and commercially available activators at 14 and 28 days.

Comparing TGA test results from samples at different curing ages (14 days and 28 days), no significant mass loss differences for activated neat fly ash were observed, whereas activated fly ash/slag blend mixes showed a significant difference. The mass loss trends at 14 days of 60/40 fly ash/slag pastes produced with WG-based and commercial activators are almost identical, whereas 28-day old pastes activated with the WG-based sodium silicate showed lower mass changes than the control sample (activated with commercially available solutions).

Total mass loss for neat fly ash specimens activated with a WG-based activator at 28 days was equal to 10%, whereas pastes produced with commercially available solutions were about 7%. When looking into fly ash/slag samples, total mass loss was equal to 17% for pastes produced with a WG-based activator at 28 days, whereas this was 20% for samples produced with commercially available solutions.

3.4. SEM/EDX Analysis of the Activated Pastes

The micrographs of alkali-activated neat fly ash and 60%/40% fly ash/slag pastes are shown in Figure 5. The WG-based activator seems to allow a satisfactory dissolution of raw materials, not hindering the polycondensation rate during the geopolymer synthesis and allowing the maximum geopolymer gel formation which is visible in Figure 5b. When commercially available activators were used, the excess OH concentration left in the system

weakened the structure of the geopolymer and reduced the uniformity of geopolymer gels. The reduced water content led to difficulty in the diffusion of dissolved species, which could hinder the polycondensation rate. Unreacted particles were observed in the microstructure, and this could explain the lower compressive strength recorded. The features visible in Figure 5a seem to confirm this interpretation. The lack of water for gel formation was more obvious in 60%/40% fly ash/slag blend activated with commercially available solutions, leading to the formation of micro-cracks resulting in increased porosity, see Figure 5c.

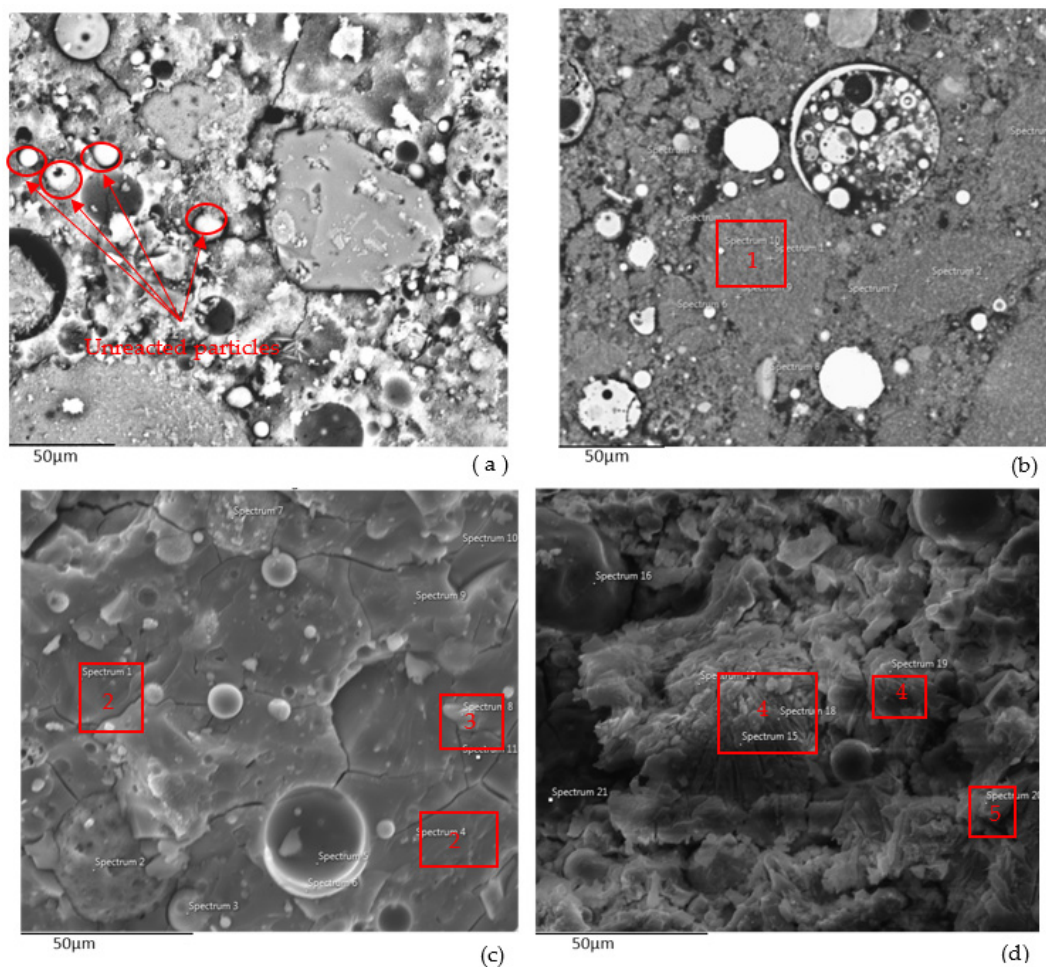


Figure 5. SEM micrographs. (a) Neat fly ash activated with commercially available solutions. (b) Neat fly ash activated with WG-based sodium silicate. (c) 60/40 fly ash/slag blends activated with commercially available solutions. (d) 60/40 fly ash/slag blends activated with WG-based sodium silicate.

EDX spectrum (Figure 5a) measured on the spherical shapes indicated the presence of Si, Al, O, and K, but not of Na, confirming that these residues are unreacted fly ash cenospheres. EDX spectra obtained from the spot indicated by red squares 1 (Figure 5b) show that these areas mainly contain Si, Al, O, and Na, whereas areas indicated by the square 2 in Figure 5c had a significant amount of Ca due to the presence of slag. These elements are the major constituents of the reacted alkali-activated matrix. Fe was detected in all the spectra, suggesting that the micro grains are likely hematite aggregates. Areas under red square 3 (Figure 5c) resulted in a lower content of Na, suggesting partially reacted particles. EDX spectra from the areas indicated by red square 4 (Figure 5d) identified mainly Si, Na, and O. These three elements are the major constituents of WG-based activator powder; thus, it can be deduced that the reaction in these areas was not complete. EDX

spectrum of the area indicated by red square 5 mainly contains Ca, Si, Na, Al, Mg, and O which are the major constituents that can be found in activated slag.

The EDX results are used to provide qualitative and quantitative evidence for the formation of geopolymer gels. The average values of Si/Al, Na/Al, Al/Na, Ca/Si, Na/Ca, and Mg/Al molar ratios, calculated from EDX results on an average of at least six points, are shown in Table 4 along with their ranges of variability.

Table 4. Range and average of chemical elements ratios based on the point analysis of SEM (EDX spectra).

| Element Ratio | 100F-70-28Days-Crushed | | FCON-28Days-Crushed | | 60/40FG-70-28Days-Crushed | | FG-CON-28Days-Crushed | |
|---------------|------------------------|---------|---------------------|---------|---------------------------|---------|-----------------------|---------|
| | Range | Average | Range | Average | Range | Average | Range | Average |
| Si/Na | 1.08–2.43 | 1.77 | 1.82–3.06 | 2.46 | 1.07–3.86 | 1.78 | 1.61–2.63 | 2.13 |
| Si/Al | 1.82–3.14 | 2.63 | 1.4–3.81 | 2.64 | 2.71–6.07 | 3.73 | 2.59–4.25 | 3.45 |
| Al/Na | 0.34–1.0 | 0.68 | 0.67–2.13 | 1.02 | 0.31–0.63 | 0.47 | 0.43–0.89 | 0.63 |
| Ca/Si | 0.09–0.25 | 0.13 | 0.03–0.13 | 0.08 | 0.60–2.87 | 1.2 | 0.64–0.90 | 0.75 |
| Na/Ca | 2.91–8.64 | 4.93 | 2.5–11.6 | 5.92 | 0.12–1.39 | 0.78 | 0.44–0.96 | 0.66 |
| Mg/Al | 0.08–0.12 | 0.09 | 0.05–0.12 | 0.09 | 0.23–0.43 | 0.35 | 0.13–0.75 | 0.33 |

The average molar ratio of Si/Al for neat fly ash control samples (i.e., activated with commercially available solutions) at 28 days was equal to 2.64, very close to the value of 2.63 calculated for samples activated with the WG-based activator. The Al/Na ratio for control samples was equal to 1.02, whereas the WG-based activated sample provided a value of 0.68. As shown in Figure 5b, the Na contents were obtained from the reacted areas seen in SEM images, which are likely to represent the geopolymer gels. Si/Al ratios of geopolymer gels reported in the literature are in the range of 2–3 [25,26].

Si/Al ratios calculated for 60%/40% fly ash/slag samples at 28 days were higher than 3, and this is presumably due to the formation of C–S–H and C–A–S–H gels, as well as due to a reduction in the amount of Al (which was provided mainly by fly ash). Although Si and Al can be detected from either fly ash, slag and geopolymer gel, the ratios can still provide qualitative indications of the nature of geopolymer gels formed through the reaction. Al/Na ratios in the range of 1.0 are the typical value of geopolymers reported in the literature [27]. Fly ash/slag blend samples displayed less incorporation of Al³⁺ ions in their main geo-polymeric phase compared to neat fly ash geopolymers, as confirmed by the lower Al/Na ratio and higher Si/Al ratio of the resultant geopolymer paste. The gel of fly ash/slag pastes activated with the WG-based silicate showed a Ca/Si molar ratio of 1.2, which is higher than the ratio of 0.75 calculated for control samples, and seems to suggest the presence of a C–S–H type gel, which is in agreement with the literature [28]. This ratio was reported to be about 1.1 in alkali-activated slag [29] and 1.2–2.3 in Portland cement [30].

4. Conclusions

Based on the results presented, the following conclusions can be drawn:

- The activator developed from glass waste can depolymerise the original silicate and/or alumina-silicate structures and be used to activate common precursors.
- In the presence of a neat fly ash precursor, the WG-based activator seemed to develop a denser structure when compared to the control (i.e., commercially available activating solutions) samples. The total mass loss of the WG-based samples was higher than that of control samples, suggesting a higher degree of reaction.
- When used with blended mixes of 60%/40% fly ash/slag, the WG-based activator seemed to produce a denser structure, especially after 28 days.

- The WG-based activator seemed more efficient at activating neat fly ash than blended fly ash/slag mixes.
- Significant reacted areas can be observed in the SEM images of WG-based activated samples, and quantitative ratios of the main chemical species confirmed the nature of N-A-S-H and C-A-S-H gels which were broadly comparable between the control samples and the WG-based activated samples, thus confirming the quality of the WG-based sodium silicate in activating the typical precursors.

Author Contributions: Conceptualization, D.B. and R.V.; methodology, D.B. and R.V.; validation, R.V.; formal analysis, D.B.; investigation, D.B.; data curation, D.B.; writing—original draft preparation, D.B.; writing—review and editing, R.V. All authors have read and agreed to the published version of the manuscript.

Funding: This research was partially funded by Innovate UK-EP SRC, United Kingdom, project RE-SCIND “REcovery and uSe of Cement kiln Dust as the alkali activator for Geopolymeric (Cementless) Concrete Building Blocks”, Grant Ref. EP/N508962/1, and Newton Fund-Low Carbon footprint Precast Concrete products for an energy efficient built environment (LowCoPreCon) Innovate UK no. 102721.

Acknowledgments: The support of Marios Soutsos, Principal Investigator of the grants that funded this research, is gratefully acknowledged. Authors are also grateful to Susan Lawther for her contribution in the sample preparation.

Conflicts of Interest: The authors declare no conflict of interest.

References

1. Siddika, A.; Hajimohammadi, A.; Mamun, A.A.; Alyouse, R.; Ferdous, W. Waste Glass in Cement and Geopolymer Concretes: A Review on Durability and Challenges. *Polymers* **2021**, *13*, 2071. [[CrossRef](#)] [[PubMed](#)]
2. Siddika, A.; Hajimohammadi, A.; Ferdous, W.; Sahajwalla, V. Roles of Waste Glass and the Effect of Process Parameters on the Properties of Sustainable Cement and Geopolymer Concrete—A State-of-the-Art Review. *Polymers* **2021**, *13*, 3935. [[CrossRef](#)] [[PubMed](#)]
3. Topçu, I.B.; Canbaz, M. Properties of concrete containing waste glass. *Cem. Concr. Res.* **2004**, *34*, 267–274. [[CrossRef](#)]
4. Ke, G.; Li, W.; Li, R.; Li, Y.; Wang, G. Mitigation Effect of Waste Glass Powders on Alkali-Silica Reaction (ASR) Expansion in Cementitious Composite. *Int. J. Concr. Struct. Mater.* **2018**, *12*, 67. [[CrossRef](#)]
5. Toniolo, N.; Rincón, A.; Roether, J.; Ercole, P.; Bernardo, E.; Boccaccini, A. Extensive reuse of soda-lime waste glass in fly ash-based geopolymers. *Constr. Build. Mater.* **2018**, *188*, 1077–1084. [[CrossRef](#)]
6. Zhang, S.; Keulen, A.; Arbi Ghanmi, K.; Ye, G. Waste glass as a partial mineral precursor in alkali-activated slag/fly ash system. *Cem. Concr. Res.* **2017**, *102*, 29–40. [[CrossRef](#)]
7. Liu, G.; Florea, M.V.A.; Brouwers, H.J.H. The role of recycled waste glass incorporation on the carbonation behaviour of sodium carbonate activated slag mortar. *J. Clean. Prod.* **2021**, *292*, 126050. [[CrossRef](#)]
8. Liu, G.; Florea, M.; Brouwers, J. Waste glass as a binder in alkali-activated slag–fly ash mortars. *Mater. Struct.* **2019**, *52*, 101. [[CrossRef](#)]
9. Moncea, M.A.; Panait, A.M.; Dumitru, F.D.; Baraitaru, A.G.; Olteanu, M.V.; Deák, G.; Boboc, M.; Stanciu, S. Metakaolin-waste glass geopolymers. The influence of hardening conditions on mechanical performances. *IOP Conf. Ser. Mater. Sci. Eng.* **2019**, *572*, 12057. [[CrossRef](#)]
10. Mácová, P.; Sotiriadis, K.; Slížková, Z.; Šašek, P.; Řehoř, M.; Závada, J. Evaluation of Physical Properties of a Metakaolin-Based Alkali-Activated Binder Containing Waste Foam Glass. *Materials* **2020**, *13*, 5458. [[CrossRef](#)]
11. Larbi, S.; Khaldi, A.; Maherzi, W.; Abriak, N.E. Formulation of Compressed Earth Blocks Stabilized by Glass Waste Activated with NaOH Solution. *Sustainability* **2022**, *14*, 102. [[CrossRef](#)]
12. Sasui, S.; Kim, G.; Nam, J.; van Riessen, A.; Eu, H.; Chansomsak, S.; Alam, S.F.; Hee Cho, C. Incorporation of Waste Glass as an Activator in Class-C Fly Ash/GGBS Based Alkali Activated Material. *Materials* **2020**, *13*, 3906. [[CrossRef](#)] [[PubMed](#)]
13. Melele, S.J.K.; Banenzoué, C.; Fotio, D.; Tchakouté1, H.K.; Rüscher, C.H.; Nansou, C.P.N. Improvement of the reactivity of soda-lime-silica glass solution as a hardener for producing geopolymer materials. *SN Appl. Sci.* **2019**, *1*, 1208. [[CrossRef](#)]
14. Bagheri, A.; Moukannaa, S. A new approach to the reuse of waste glass in the production of alkali-activated materials. *Clean. Eng. Technol.* **2021**, *4*, 100212. [[CrossRef](#)]
15. Vinai, R.; Soutsos, M. Production of sodium silicate powder from waste glass cullet for alkali activation of alternative binders. *Cem. Concr. Res.* **2019**, *116*, 45–56. [[CrossRef](#)]
16. Samarakoon, M.H.; Ranjith, P.G.; Duan, W.H.; De Silva, V.R.S. Properties of one-part fly ash/slag-based binders activated by thermally-treated waste glass/NaOH blends: A comparative study. *Cem. Concr. Compos.* **2020**, *112*, 103679. [[CrossRef](#)]

17. Figueiredo, R.A.; Brandão, P.R.; Soutsos, M.; Henriques, A.B.; Fourie, A.; Mazzinghy, D.B. Producing sodium silicate powder from iron ore tailings for use as an activator in one-part geopolymer binders. *Mater. Lett.* **2021**, *288*, 129333. [[CrossRef](#)]
18. Vinai, R.; Ntimugura, F.; Cutbill, W.; Evans, R.; Zhao, Y. Bio-derived sodium silicate for the manufacture of alkali activated binders: Use of bamboo leaf ash as silicate source. *Int. J. Appl. Ceram. Technol.* **2022**, *19*, 1235–1248. [[CrossRef](#)]
19. Abdulkareem, M.; Havukainen, J.; Nuortila-Jokinen, J.; Horttanainen, M. Environmental and economic perspective of waste-derived activators on alkali-activated mortars. *J. Clean. Prod.* **2021**, *280*, 124651. [[CrossRef](#)]
20. Bianco, I.; Tomos, B.A.D.; Vinai, R. Analysis of the environmental impacts of alkali-activated concrete produced with waste glass-derived silicate activator—A LCA study. *J. Clean. Prod.* **2021**, *316*, 128383. [[CrossRef](#)]
21. Uchino, T.; Sakka, T.; Lwasak, M. Interpretation of Hydrated States of Sodium Silicate Glasses by Infrared and Raman Analysis. *J. Am. Ceram. Soc.* **1991**, *74*, 306–313. [[CrossRef](#)]
22. Lee, W.K.W.; Van Deventer, J.S.J. Use of infrared spectroscopy to study geo-polymerisation of heterogeneous amorphous alumina silicates. *Langmuir* **2003**, *19*, 8726–8734. [[CrossRef](#)]
23. Bondar, D.; Lynsdale, C.J.; Milestone, N.B.; Hassani, N.; Ramezaniapour, A.A. Effect of type, form and dosage of activators on strength of alkali-activated natural pozzolans. *Cem. Concr. Compos.* **2011**, *33*, 251–260. [[CrossRef](#)]
24. Al-Majidi, M.H.; Lampropoulos, A.; Cundy, A.; Meikle, S. Development of geopolymer mortar under ambient temperature for in situ applications. *Constr. Build. Mater.* **2016**, *120*, 198–211. [[CrossRef](#)]
25. Mohammed, B.S.; Haruna, S.; Wahab, M.M.A.; Liew, M.S.; Haruna, A. Mechanical and microstructural properties of high calcium fly ash one-part geopolymer cement made with granular activator. *Heliyon* **2019**, *5*, e02255. [[CrossRef](#)]
26. Davidovits, J. Properties of geopolymer cement. In Proceedings of the First International Conference on Alkaline Cement and Concretes, Kiev, Ukraine, 11–14 October 1994.
27. Rowles, M.R.; O'Connor, B.H. Chemical and structural microanalysis of aluminosilicate geopolymers synthesized by sodium silicate activation of metakaolinite. *J. Am. Ceram. Soc.* **2009**, *92*, 2354–2361. [[CrossRef](#)]
28. Bondar, D.; Lynsdale, C.J.; Milestone, N.B.; Hassani, N.; Ramezaniapour, A.A. Effect of adding mineral additives to alkali-activated natural pozzolan paste. *Constr. Build. Mater.* **2011**, *25*, 2906–2910. [[CrossRef](#)]
29. Brough, A.R.; Atkinson, A. Sodium silicate-based, alkali-activated slag mortars: Part, I. Strength, hydration and microstructure. *Cem. Concr. Res.* **2002**, *32*, 865–879. [[CrossRef](#)]
30. Richardson, I.G. The nature of C-S-H in hardened cements. *Cem. Concr. Res.* **1999**, *29*, 1131–1147. [[CrossRef](#)]